Available online at www.sciencedirect.com
ScienceDirect
Journal of Power Sources 172 (2007) 416–421
JOURNAL OF POWER SOURCES
www.elsevier.com/locate/jpowsour

Short communication

Lithium-ion batteries with high charge rate capacity: Influence of the porous separator

D. Djian [a], F. Alloin [b,*], S. Martinet [a], H. Lignier [a], J.Y. Sanchez [b]

[a] *CEA-LITEN, 17 rue des martyrs, 38054 Grenoble Cedex 9, France*
[b] *Laboratoire d'Electrochimie et de Physico-chimie des Matériaux et des Interfaces-LEPMI, UMR 5631 CNRS-INPG-UJF, BP 75, 38402 Saint-Martin-d'Hères Cedex, France*

Received 28 February 2007; received in revised form 12 June 2007; accepted 8 July 2007
Available online 17 July 2007

Abstract

The performance of commercial separators at high charge rates was evaluated using $Li_4Ti_5O_{12}$ and $LiMn_2O_4$ as negative and positive electrodes, respectively. Most of the porous separators tested induced a sharp decrease in the conductivity of the liquid electrolyte. The conductivity decrease was related to the amount of porosity, polymer/electrolyte affinity, and the size of the pores and their interconnection. The decrease in conductivity induced by the separator incorporation and the separator thickness seems to be relevant indicators for optimizing a separator dedicated to high charge rate lithium-ion batteries.

Keywords: $Li_4Ti_5O_{12}$; Polyolefin; Lithium-ion battery; High charge rate

1. Introduction

Due to growing energy storage needs for current consumer markets, e.g. 4C market and hybrid vehicles and for future markets as electrical vehicles, there is an increasing demand for high performance electrochemical energy sources such as fuel cells and batteries. The main advantages of lithium-based power sources are their light weight and their very high specific energy. Their disadvantages are their lower power densities and their poor tolerance of high charge rates.

The rate capability limitation of lithium-ion batteries results from several factors, including the battery design and used materials. The solid-state diffusion of lithium ions in the active electrode materials [1], the charge transfer kinetics reaction, the concentration gradient either in the porous electrodes or in the electrolyte, the ionic conductivity in the electrolyte or in the porosity of the electrode, or the electrode electronic conductivity may be the limiting processes [2,3]. Furthermore, the limiting processes depend notably of the charge and discharge rates. In order to increase the solid-state diffusion of lithium in active material, in particular to improve rate capabilities, intensive studies have been performed on new nanostructured electrode materials [4]. Optimization, both of the thickness and of the porosity of the electrodes may be also performing to improve the high rate performance [3].

Carbon materials have been used predominantly as lithium-ion battery anodes. While graphite can be used for high discharge rates, it is not recommended for high charge rates. Indeed, at high charge rates, metallic lithium deposits have been observed on the graphite surface, leading to dendrite formation. $Li_4Ti_5O_{12}$ is a negative electrode material that can be used as an alternative to graphite for fast charge Li-ion systems [5,6].

The interest of this material lies in the fact that at high charge rates, lithium dendrite formation is impossible thanks to the high potential of $Li_4Ti_5O_{12}$. Thus, the use of appropriate positive and negative electrodes fulfilling criteria as thickness, porosity, active material, may allow high charge rates to be achieved.

In this paper, we evaluate the behaviour of commercial separators at high charge rates using $Li_4Ti_5O_{12}$ and $LiMn_2O_4$ as negative and positive electrodes, respectively. In order to highlight the influence of the separator on the secondary battery performances, the positive electrode was used in large excess while very thin and highly porous electrodes were used as negative electrode. The morphology of commercial separators,

* Corresponding author. Tel.: +33 4 76 82 65 60; fax: +33 4 76 82 65 77.
E-mail address: Fannie.alloin@enseeg.inpg.fr (F. Alloin).

0378-7753/$ – see front matter © 2007 Elsevier B.V. All rights reserved.
doi:10.1016/j.jpowsour.2007.07.018

i.e. porosity, structure, conductivity behaviour of the set electrolyte + separator combination, and electrochemical response during high charge rates were evaluated.

2. Experimental details

2.1. Commercial macroporous separators

The macroporous polyolefin separators were provided by Celgard Inc.: Celgard® 2400, Celgard® 2500, Celgard® 2730 and DSM Solutech: Solupor® 3P07A, Solupor® 10P05A and Solupor®14P01A. The Celgard® separators are made by a dry process. The melted polymer is extruded and stretched in only one direction [7], giving a separator that is relatively thin (<75 μm) and with porosity lower than 50%. The DSM separators are obtained by a wet process. The polymers are extruded in a gel form and stretched in two directions. The resulting separators have thicknesses ranging from 10 μm to 60 μm and porosities up to 80%.

2.2. Liquid electrolyte

The experimental liquid electrolyte was LP30® manufactured by Merck. The electrolyte used was a molar solution of $LiPF_6$ in a 1/1 (w/w) mixture of ethylene carbonate (EC) and dimethyl carbonate (DMC). The electrolyte was stored in a glove box under dry argon.

2.3. Electrode

The positive electrode consisting of a manganese spinel ($LiMn_2O_4$) was a commercial grade purchased from Erachem. The insertion potential of this material is 4.1 V versus Li/Li^+ and its specific capacity is 120 mAh g^{-1} [8]. The electroactive material for the negative electrode was a home-made lithiated titanium oxide $Li_4Ti_5O_{12}$ with a lithium insertion potential of 1.55 V versus Li/Li^+ and a specific capacity equal to 160 mAh g^{-1} [9]. The composite electrodes were prepared by blending $Li_4Ti_5O_{12}$ and $LiMn_2O_4$ powder with 6% acetylene black, 6% of carbon fibrous and 6% of poly(vinylidene fluoride) (PVdF, Solef® 1015, Solvay). The current collectors were 20 μm thick aluminium foil. The thicknesses of the electrodes were 20 μm and 80 μm for negative and positive electrodes, respectively. The area capacity densities were 1.7 ± 0.1 mAh cm^{-2} and $0.4(\pm 0.05)$ mAh cm^{-2} for the positive and negative electrodes, respectively. The area capacity density of each cell was determined with a good accuracy; the precision of the measurement was about 3%. The electric percolation, the porosity volume and the adhesion of the electrodes on the aluminium foil were achieved by compression. The resulting electrodes were dried under vacuum at 80 °C for 48 h.

2.4. Pore diameter measurements

All measurements were carried out over the pressure range 0.6×10^5 Pa to 410×10^5 Pa using a Micrometrics® Autopore IV 9200 series.

The pore diameters were measured by intrusion and extrusion of mercury. The pore diameter distribution, the pore shape and the porous structure interconnectivity were determined using the Laplace equation (1):

$$R = -\frac{2\gamma \cos(\theta)}{\Delta P} \quad (1)$$

where R is the pore diameter, ΔP the mercury pressure, γ the surface tension equal to 480×10^{-5} N cm^{-1} and θ is the contact angle equal to 130° for all samples.

2.5. Gas permeability measurements

The gas permeability measurements were performed in dry air on a laboratory-made set-up. The permeability coefficient B of the samples was calculated according to Darcy's law (2) in which l is the separator thickness, μ (Pa s) the air viscosity, ΔP (Pa) the differential pressure through the separator and v (m s^{-1}) the velocity of the gas. ΔP was measured through the controlled velocity of air. The diameter of the samples was 26 mm:

$$B = \frac{l\mu v}{\Delta P} \quad (2)$$

2.6. Ionic conductivity measurements

Conductivity measurements were carried out in CR2032 coin cells assembled and sealed in a glove box under dry argon (<2 ppm H_2O). The metallic components were dried under vacuum at 120 °C for 48 h. Blocking electrodes were made from 16 mm diameter stainless steel. The cell constant was determined using KCl solution in Viledon® separator with a good accuracy and was found in accordance with the electrode area and the thickness of the sample. All measurements were performed three times, with a good accuracy about 15%, using impedance spectroscopy over the frequency range 1 Hz–1.3 MHz with ±10 mV amplitude around the OCV, using a Solartron SI 1260 analyser equipped with a Solartron SI 1287 interface.

2.7. Cycling test

The cycling tests were performed on an Arbin® multichannel system, using CR2032 coin cells first sealed in a glove box under dry argon. A stainless steel disc and a spring ensured the cohesion of the system.

The cycling tests were performed in galvanostatic mode. The cut-off limits were related to the voltage of the battery: 2.9 V in charge, 1 V and 1.5 V for high or low discharge rates, respectively. These voltage limits were used to prevent over-discharge and over-charge. The charge/discharge yield was close to 100% even at high charge rates. The experiments were performed several times for each battery and each charge rate.

3. Results and discussion

The manufacturing process of the separator governs the porous structure and mechanical behaviour.

Table 1
Thickness, porosity, permeability coefficient B, median diameters determined by mercury porosimetry, d_m, and permeability pore diameter, d_p, of commercial macroporous separators

Porous separator	Thickness (μm)	Porosity (%)	Porosity Hg (%)	d_m (μm)	d_p (μm)	B ($\times 10^{-14}$ m^2)
Celgard® 2400	24	32	31	0.1		
Celgard® 2500	23	47	53	0.2		
Celgard® 2730	17	27	39	0.1		
Solupor® 14P01A	23	40	44	0.3	1	0.5
Solupor® 3P07A	13	70	72	1.3	1.1	1.3
Solupor® 10P05A	57	78	80	2.2	1.7	2.9

Porosity Hg is determined by mercury porosimetry.

3.1. Macroporous structure of commercial separators

The thickness and porosity of the separators are shown in Table 1. Porosity was determined using (i) the weight and size of the sample in relation to the density of the material and (ii) the mercury porosity technique. The measured porosities obtained by both techniques were very close except for the Celgard® 2730 separator. Solupor® 3P07A and Solupor® 10P05A showed the highest porous volumes.

Due to an anisotropic manufacturing process, i.e. Celgard® extrusion technique, pores are lengthened and orientated in the same direction (Fig. 1). The separator is a crystalline polyolefin, i.e. polypropylene or polyethylene [10].

The Solupor® separators, based on ultra-high molecular weight polyethylene, present a fibrous network with a large pore structure (Fig. 2). The difference compared with the former porous structure results from the manufacturing processes, namely dry unidirectional stretching for the Celgard® separators and wet bidirectional stretching for the Solupor® ones.

A difference was found between the mercury intrusion behaviour (Fig. 3) with the Celgard® separators and the Solupor® separators. Intrusion in the Celgard® separators started at a threshold corresponding to measured pore diameters of close to 0.3 μm, whereas the intrusion began at low pressure in the case of the Solupor® separators. This behaviour led to a wider pore diameter distribution in Solupor® separators than in Celgard® ones. Fig. 4 shows the pore distribution curves for the Celgard® 2500 and Solupor® 10P05A separators. The Celgard® 2500 curve shows a narrow distribution in pore diameter centred on 0.19 μm while the Solupor® 10P05A one is broader and exhibits several pore diameter distributions. Moreover, the pore diameters are larger for the Solupor® separators than for the Celgard® ones. This trend could be characterized with the median diameter, which corresponds to 50% of the mercury vol-

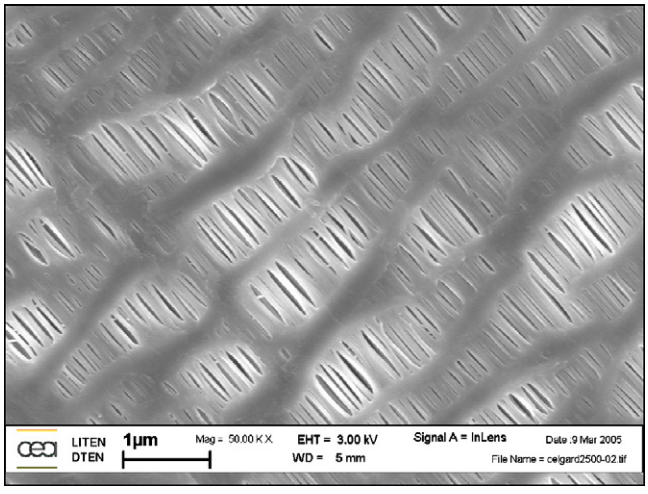

Fig. 1. SEM of the commercial macroporous separator Celgard® 2500 surface (SEM-FEG, 50,000×).

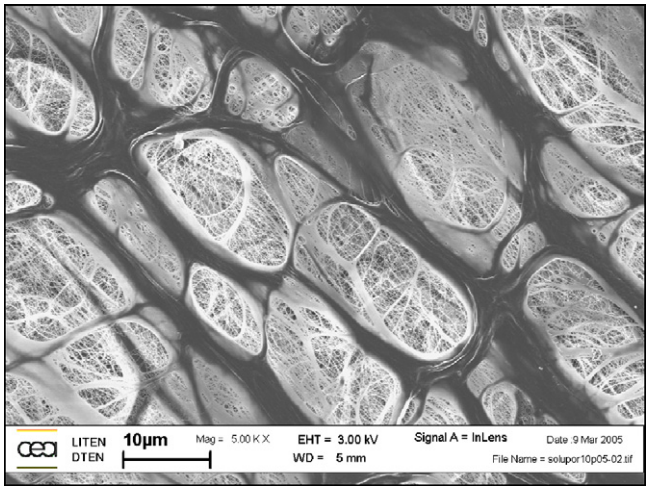

Fig. 2. SEM of the commercial macroporous macroseparator Solupor® 10P05A surface (SEM-FEG, 5000×).

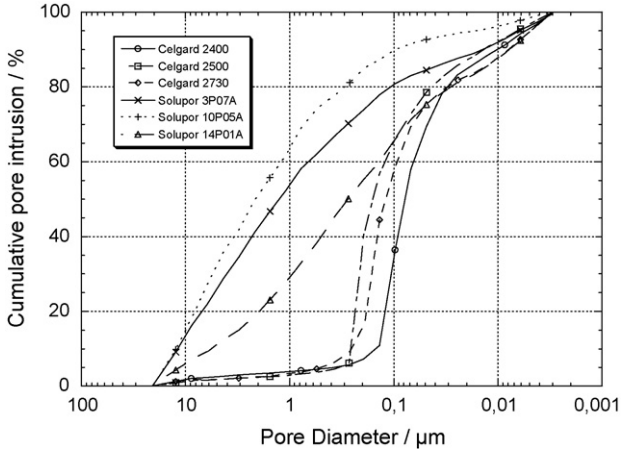

Fig. 3. Intrusion of mercury in the Celgard® and Solupor® separators.

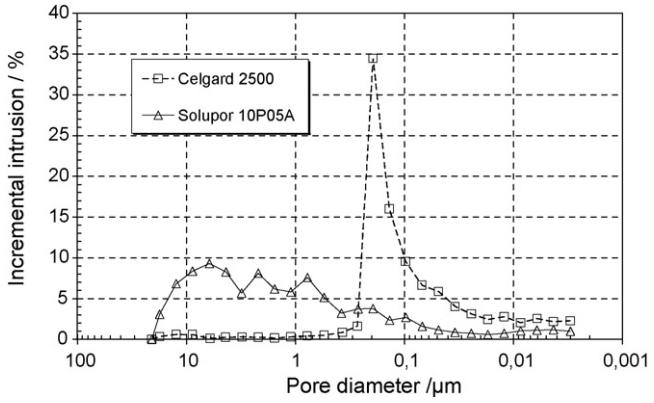

Fig. 4. Pore diameter distribution for the Celgard® 2500 and the Solupor® 10P05A separators.

ume penetration in the sample (Table 1). The mercury intrusion versus pore diameter exhibited an intermediate behaviour in the case of Solupor® 14P01A, in relation with the presence of small pore and large pore diameter distributions.

The structure of the Solupor® (Fig. 2) is in accordance with the wide distribution of pore diameters observed by mercury porosimetry.

Gas permeability tests were used to calculate the pore diameters d_p, (3) from the permeability coefficient B, porosity and the Kozeny constant h_k:

$$d_p = 4\sqrt{\frac{h_k B}{\varepsilon_p}} \tag{3}$$

The Kozeny constant depends on the porous structure, the shape and the tortuosity of the pores. It is assumed for the studied porosities that h_k is equal to 5, this value being proposed for a stacking up of isomeric particles which develop porous volume between 0.6 and 0.8 [11]. The results are gathered in Table 1.

For the Solupor® samples, the pore diameters obtained using both techniques (mercury porosimetry and gas permeability tests) followed similar evolution, i.e. the classification of Solupor® samples versus pore diameter is the same. The difference between pore diameter values is due to assumptions in both techniques, i.e. model used for porous structure. In the same experimental conditions, Celgard® separators were found impermeable to air which might be related to their small pore diameters.

3.2. Conductivity characterization

Macroporous separators are intended to prevent shorts but they sharply decrease the ionic conductivity of liquid electrolytes. Parameters such as the MacMullin number N_M [12–14] and tortuosity τ [15] are used to characterize this behaviour. Both are defined by Eqs. (4) and (5):

$$N_M = \frac{\sigma_0}{\sigma_{eff}} \tag{4}$$

$$\sigma_{eff} = \sigma_0 \frac{\varepsilon}{\tau^2} \tag{5}$$

Table 2
Effective conductivity, MacMullin number and tortuosity of LP30® + separator

Porous separator	Porosity Hg (%)	σ_{eff} (mS cm^{-1})	N_M	τ
Celgard® 2400	31	0.6 ± 0.08	16 ± 2	2.3
Celgard® 2500	53	0.8 ± 0.1	13 ± 1.5	2.5
Celgard® 2730	39	0.9 ± 0.1	11 ± 1.2	2.1
Solupor® 14P01A	44	0.4 ± 0.04	22 ± 2	3.3
Solupor® 3P07A	72	0.7 ± 0.08	13 ± 1.5	3.2
Solupor® 10P05A	80	2.1 ± 0.1	5 ± 0.2	1.9

$\sigma_0 = 9.8$ mS cm^{-1} at 21 °C.

where σ_0 is the conductivity of pure liquid electrolyte, σ_{eff} the conductivity of the separator + liquid electrolyte combination, and ε is the porosity ratio.

The conductivity measurements were performed using LP30® liquid electrolyte, EC/DMC (50/50 v/v) 1 M $LiPF_6$ ($\sigma_0 = 9.8$ mS cm^{-1}). The results are provided in Table 2.

The MacMullin numbers, N_M, exceeds 10, except for Solupor® 10P05A. These high values are associated with a sharp conductivity decrease related (i) to the porosity structure and (ii) to the poor affinity between polyolefin and the polar electrolyte. The best conductivity values, which were obtained with Solupor® 10P05A, might be related to its high porous volume and large pore diameter.

The highest N_M, i.e. lowest conductivity, was obtained, in accordance with its low porous volume, for Solupor® 14P01A. Surprisingly, despite their close porous volume, the electrolyte + Celgard® combinations had lower N_M numbers, i.e. higher conductivity, than the electrolyte + Solupor® 14P01A. This might be related to the uniaxial orientation of Celgard® separators, whose macroporous structure is perpendicular to the film surface.

Furthermore, in the Celgard® series, no direct correlation can be seen between porosity ratio or pore diameter and N_M. Indeed, the honeycomb structure of commercial separators leads to complex transport ways where the interconnectivity of pores and therefore the tortuosity become relevant parameters.

The tortuosity values, determined using (5), might explain the lower conductivities obtained with Solupor® 14P01A than with Celgard® (Table 2). Indeed, the tortuosity makes it possible to take into account the impact of the macroporous structure on conductivity.

Our results, except for Celgard® 2500, are in agreement with those reported by Patel et al. [14] who measured the N_M of Celgard® 2400, 2500 and Solupor® 14P01A using EC/DEC (1/1 wt%) + $LiPF_6$ 1 M electrolyte, Abraham et al. [13], using THF (Tetrahydrofurane) + $LiAsF_6$ 1.5 M electrolyte, found a $N_M = 23$ for Celgard® 2400. This difference in N_M values might be related to different affinities between separator and electrolyte. The latter might induce a difference in wetting behaviour.

3.3. Battery characterization

The performance of the secondary battery, $Li_4Ti_5O_{12}$/electrolyte/$LiMn_2O_4$ and commercial macroporous separators, was investigated by cycling tests performed at different

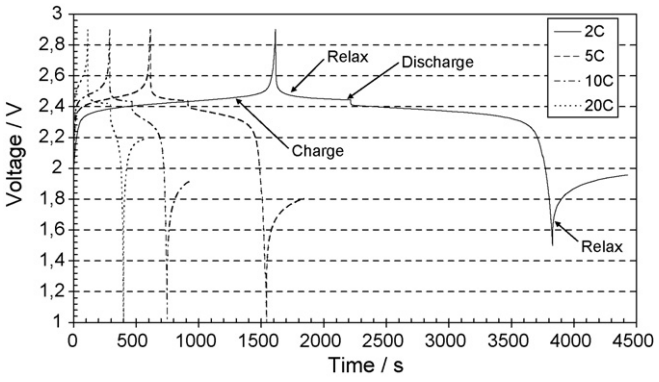

Fig. 5. Voltage profile vs. time for several charge rates for $Li_4Ti_5O_{12}$/LP30® + Celgard® 2500/$LiMn_2O_4$ battery. The relaxation process is performed for a 5-min period.

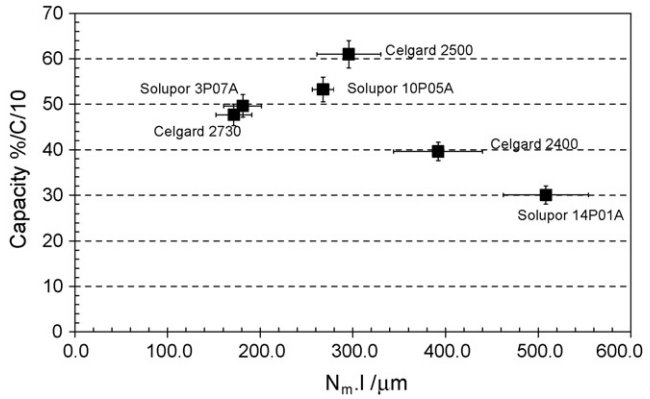

Fig. 7. Specific capacities charged at 20*C* for different the $N_M l$ factors for $Li_4Ti_5O_{12}$/electrolyte/$LiMn_2O_4$.

charge rates. The charge rates used were between *C*/10 (10 h, 0.04 mA cm^{-2}) and 20*C* (3 min, 8 mA cm^{-2}). The voltage profile versus time using several charge rates is given for $Li_4Ti_5O_{12}$/LP30® + Celgard® 2500/$LiMn_2O_4$ battery in Fig. 5. An excess of $LiMn_2O_4$ led to a stable potential on a wide range of charge rates.

To better compare the separators, the charging capacities were normalized using those obtained at a low charge rate, *C*/10. The results are presented as a function of charge rate in Fig. 6.

For low charge rates, the electrochemical performance of the different batteries is roughly similar, the capacities being equal to 140 ±5 mAh g^{-1}. From these data it can be inferred that the separator morphology has no significant effect on the battery performances. In these experimental conditions, ionic mobility in the electrolyte (liquid + separator) cannot be identified to a limiting process.

On the contrary, the charge capacity obtained at the highest charge rate, 20*C*, notably depends on the used separator. Performance seems to depend strongly on the porous structure of the separator, the transport processes in the electrolyte seems to become, in some secondary battery tested, the limiting process. Thus, ohmic drop, associated to ionic conductivity, but also ion concentration gradient occurring at the bulk electrolyte and in the electrolyte inside the electrode might exert a large influence on the electrochemical performance of the battery.

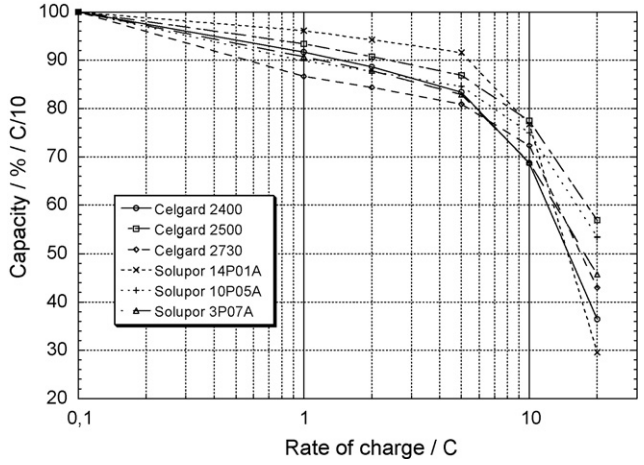

Fig. 6. Normalized capacities for different charge rates.

Optimizing high rate performance, requires an optimization both of the electrode and of the electrolyte. Thus, the overall separator/electrolyte resistance has to be minimized. For a given electrolyte, this could be achieved by minimizing separator thickness and N_M. To characterize this behaviour, Patel et al. [14] recommend using the $N_M l$ factor, where N_M is the MacMullin number previously defined and *l* is the thickness of the separator.

The highest performances, at high charge rates, were obtained with secondary batteries whose $N_M l$ factor are the lowest (Fig. 7), in accordance with Patel et al. study [14]. Capacities higher than 80 mAh g^{-1} were obtained at 20*C* for battery incorporating Celgard® 2500 as separator.

For a $N_M l$ factor higher than 300 μm, i.e. batteries using Celgard® 2400 and Solupor® 14P01A separators, the capacities obtained were lower. The capacity loss at 20*C* may be due to the structure of the separator used, i.e. porosity, thickness and pore structure, which decreases ionic mobility. At a fixed thickness, a less conductive electrolyte results in an increase of the ohmic drop and of the ion concentration gradient in the electrolyte. Indeed, the ionic mobility decrease induces the decrease of the diffusion coefficient, i.e. the Nernst–Einstein relation, thus an increase in the ion concentration gradient.

4. Conclusions

Celgard® and Solupor® commercial macroporous separators were investigated. These separators have different porous structures. The influence of the separator used on the electrolyte resistivity and on the battery capacity at high rate capacities was evaluated. Most of the commercial porous separators induced a sharp decrease in the conductivity of the liquid electrolyte. This conductivity decrease may be associated with the amount of porosity, the polymer/electrolyte affinity, the size of the pores and their interconnection. The $N_M l$ factor of the separators seems to be a relevant indicator to define a good electrolyte adapted to high charge rate. In a second paper, a similar analysis will be performed on macroporous separators prepared by phase inversion from poly(vinylidene fluoride) polymer.

Acknowledgments

The authors would like to thank the CNRS and the CEA, which awarded a grant to Damien Djian.

References

[1] P.R. Bueno, E.R. Leite, J. Phys. Chem. 107 (2003) 8868–8877.
[2] J. Newman, J. Electrochem. Soc. 1 (1995) 97–101.
[3] S. Atlung, W. West, J. Power Sources 26 (1989) 139–159.
[4] C.R. Sides, C.R. Martin, Adv. Mater 17 (2005) 125–128.
[5] A.N. Jansen, A.J. Kahaian, K.D. Kepler, P.A. Nelson, K. Amine, D.W. Dees, D.R. Vissers, M.M. Thackeray, J. Power Sources 81–82 (1999) 902–905.
[6] F. Orsini, A. du Pasquier, B. Beaudouin, J.M. Tarascon, M. Trentin, N. Langenhuizen, E. de Beer, P. Notten, J. Power Sources 81–82 (1999) 918–921.
[7] G. Venugopal, J. Moore, J. Howards, S. Pendalwar, J. Power Sources 77 (1999) 34–41.
[8] D. Guyomard, J.-M. Tarascon, J. Electrochem. Soc. 139 (1992) 937–948.
[9] K. Nakahara, R. Nakajima, T. Matsushima, H. Majima, J. Power Sources 117 (2003) 131–136.
[10] T. Sarada, L.C. Sawyer, M.I. Ostler, J. Membr. Sci. 15 (1983) 97–113.
[11] P.C. Carman, Trans. Inst. Chem. 15 (1937) 150–166.
[12] D.L. Caldwell, K.A. Poush, US Patent 4 464 238 (1984).
[13] K.M. Abraham, Electrochim. Acta 38 (1993) 1233–1248.
[14] K.K. Patel, J.M. Paulsen, J. Desilvestro, J. Power Sources 122 (2003) 144–152.
[15] F.L. Tye, J. Power Sources 9 (1983) 89–100.